Applied Catalysis B: Environmental 176–177 (2015) 374–384

Contents lists available at ScienceDirect

Applied Catalysis B: Environmental

journal homepage: www.elsevier.com/locate/apcatb

Investigation of co-effect of 12-tungstophosphoric heteropolyacid, nickel citrate and carbon-coated alumina in preparation of NiW catalysts for HDS, HYD and HDN reactions

P.A. Nikulshin[a,*], P.P. Minaev[a], A.V. Mozhaev[a], K.I. Maslakov[b], M.S. Kulikova[a], A.A. Pimerzin[a]

[a] Samara State Technical University, 244 Molodogvardiyskaya St., Samara 443100, Russia
[b] Chemistry Department, M.V. Lomonosov Moscow State University, 1-3 Leninskiye Gory, Moscow 119991, Russia

ARTICLE INFO

Article history:
Received 24 December 2014
Received in revised form 29 March 2015
Accepted 6 April 2015
Available online 8 April 2015

Keywords:
Hydrodesulphurization
Hydrogenation
Hydrodenitrogenation
Heteropolyanion
Alumina-activated carbon
Citric acid
NiW catalysts
NiWS
DBT
Naphthalene

ABSTRACT

Effects of activated carbon in a carbon-coated alumina (CCA) support, active phase morphology and its composition of Ni_6-$PW_{12}S/C_x/Al_2O_3$ catalysts in hydrotreating of model compounds were studied. The catalysts were synthesized using 12-tungstophosphoric heteropolyacid, nickel citrate and CCA and characterized with multiple methods: N_2 physisorption, X-ray powder diffraction, H_2 temperature programmed reduction, temperature-programmed desorption of ammonia, high-resolution transmission electron microscopy and X-ray photoelectron spectroscopy. The catalytic properties were determined using a fixed-bed microreactor in hydrotreating of dibenzothiophene, naphthalene and quinoline. It was found that with the increase of carbon content in the CCA up to 5 wt.%, reducible reactivity, sulphidation degree, average length and stacking number of WS_2 crystallites in the catalysts increased. Observed changes can be explained by weakening interaction between metal oxide species and carbon-coated support. Full promotion of the NiWS edges by nickel was achieved in the catalysts supported on the CCA with carbon content equal 0.3 wt.% and more. Activities of the catalysts in dibenzothiophene hydrodesulphurization, naphthalene hydrogenation and quinoline hydrodenitrogenation were essentially depended on the carbon content in the CCA-support. Ni_6-$PW_{12}S/C_1/Al_2O_3$ catalyst showed maximal conversions of the substrates in studied reactions. This result was achieved due to an optimal balance between turnover frequency value of the active sites and their content.

1. Introduction

Production of clean fuels with less than 10 ppm sulfur content is one of the most important problem in recent petroleum refinery [1]. In years to come, hydrotreating will remain the largest scale process of petroleum refining, and its role will continue to grow in view of ever tightening requirements on sulfur content standards in motor fuels and owing to increase of depth of petroleum refining and the involvement of unconventional hydrocarbon resources (oil shales, bituminous oils, bio-raw materials, etc.) into the hydroprocessing. These trends require more active catalysts, thus spurring intensive research both in industry and academia.

Traditionally, the binary CoMo and NiMo sulphides have attracted more attention for hydrotreating applications [1,2]. It is well known that nitrogen-containing and aromatic compounds present in feedstocks have inhibiting effects on the hydrodesulphurization (HDS) reactions [1–4]. NiW based hydrotreating catalysts having outstanding catalytic actions in hydrogenation (HYD) and hydrodenitrogenation (HDN) reactions especially at severe conditions and, therefore, attract great attention of scientists [1,2,5,6].

The catalytic synergism of $Ni(Co)Mo(W)/Al_2O_3$ catalysts is attributed to the formation of CoMoS or NiMo(W)S phases where highly dispersed $Mo(W)S_2$ crystallites are decorated with Ni or Co, which act as promoter [2]. Since the specific activity of type II active phase is remarkably higher than that of type I [2,3], various methods have been tried to design and prepare well-dispersed type II active phase on different supports. These methods employ organic chelating agents [7–10], novel or modified alumina supports that weakly interact with the active phase [11–13], or novel chemical compositions as precursors, including heteropolycompounds of Anderson and Keggin types and their derivatives [14–26].

* Corresponding author. Tel.: +7 846 242 3580; fax: +7 846 242 3580.
E-mail address: P.A.Nikulshin@gmail.com (P.A. Nikulshin).

http://dx.doi.org/10.1016/j.apcatb.2015.04.011
0926-3373/

The support type plays an essential role in determining the catalytic activity, stability, composition, and morphology of active phase particles [14,27–29]. Alumina is a commonly used support for commercial catalysts due to its relatively high surface areas, easily controlled pore structure, high packing density, thermal stability, physical strength, and recoverability [30]. However, alumina supports strongly interact with metal oxide precursors and, therefore, hinder their sulphidation. This negative effect is especially important in the case of NiW/Al_2O_3 catalysts. Sulphidation of tungsten proceeds at a lower rate in NiW/Al_2O_3 than that of molybdenum in alumina-supported CoMo or NiMo. The explanation is often reported to be the relatively strong W—O—Al bond [32]. Alternatively, Van der Vlies et al. [33,34] have found that the W—O bond is stronger than the Mo—O bond, consequently requiring higher temperatures to fully transform WO_3 to WS_2. In addition, the differences in sulphidation behavior between NiMo/Al_2O_3 and NiW/Al_2O_3 catalysts are closely related to the Ni and Mo (or W) impregnated precursors influencing the final formation of NiWS or NiMoS active phases [31–34].

Carbon as a support is reportedly preferable to alumina because of its high surface area and low acidity [29,35–37]. Besides, carbon-supported active sulphide phase can be well dispersed and it is also better to form more active Co(Ni)Mo(W)S-II phase [29,38–43]. As a result, C-supported catalysts are usually more active than those supported on alumina [27,31,41–43]. However, carbon supports have a significant disadvantage: their low packing density, which limits their application in commercial hydrotreating catalyst formulations. To make carbon materials more efficient, they are used with a binder [44–47] or deposited on another support, such as alumina [48–52] or zeolite [53]. Hydrotreating catalysts with C-modified alumina supports, reportedly, exhibit higher catalytic activity [44,45,51,52,54,55] and stability [51] than similar formulations with alumina-only supports in hydrotreating of commercial feedstocks. This effect has been attributed to incorporation of carbon into alumina, which results in a higher average stacking number of Co(Ni)MoS [52,54] and NiWS [53,55] active phases.

As found earlier with the use of TPR measurements [54] carbon-coated alumina (CCA) can accumulate gas phase hydrogen and could be a source of hydrogen for HDS and HYD reactions. Carbon affects Co(Ni)MoS active phase morphology [53,54]: by changing the carbon content it is possible to vary a stacking number/linear size ratio of the active phase particles and, thereby, to control HYD/DDS selectivity. Li et al. [55] studied NiW/CCA catalysts prepared from conventional precursors (nickel nitrate and ammonium metatungstate) with adding citric acid. They concluded that citric acid did not act as a chelating agent in the impregnation solution at a low pH (about 1.5). A beneficial role of a citric acid was classified as: (1) partly changing into carbonaceous deposits during sulphidation, which may isolate and decrease the WS_2 slab length; (2) reacting with basic and neutral OH groups to moderate the interaction between the active phase and the alumina support. Recently we found [56,57] that simultaneous using of Co_2Mo_{10} heteropoly-acid (HPA) and Co citrate complex as precursors led to the formation of highly active CoMo catalysts for deep diesel hydrotreating with MoS_2 species full decorated with Co. In opposite to [55] it was shown that the role of citric acid inferred in delaying promoter sulphidation with selective formation of CoMoS sites [58]. This result was achieved due to simultaneous usage of Mo based HPA and cobalt citrate. Unfortunately, so far the examples of simultaneous usage of W based HPA and nickel (cobalt) citrate have not been given in the open literatures. Moreover, a comprehensive study of the possible effect of intermediate carbon carrier in the CCA-supported NiW catalysts has not been given yet. Therefore, the objective of this work was to investigate the co-effect of 12-tungstophosphoric HPA, nickel citrate and CCA in preparation of NiW catalysts for HDS, HYD and HDN reactions. The HDS of dibenzothiophene (DBT), HYD of naphthalene and HDN of quinoline were the reactions selected to evaluate the catalytic properties of the materials. The results of this study should provide a better understanding the W based catalysts' structure and their HDS, HYD and HDN performances.

2. Experimental

2.1. Preparation of supports and catalysts

γ-Alumina was prepared by peptization of AlOOH boehmite TH60 (Sasol Company, Germany) with concentrated nitric acid (acid modulus 0.04) and further molding by extrusion. The extrudates were dried at 110 °C for 4 h and calcined under air at 550 °C for 2 h.

A synthesis of CCA supports was carried out by the pyrolysis of a mixture of *iso*-propanol with glycerin (2 vol.%) on alumina in a bench-scale flow reactor at 600 °C in N_2 atmosphere during 1.5–2 h. The coke content in the CCA supports was determined by quantitative oxidation to CO_2 followed by the gas-chromatographic analysis. The composition and characteristics of the prepared CCA supports are presented in Table 1. The chosen carbon amount was varied up to 5.1 wt.% [54]. Our evaluations showed that the monolayer coverage of alumina could be achieved at 5 wt.% of the carbon content.

Before impregnation, the supports were crushed and sieved to particles between 0.25 and 0.50 mm. The Ni_6-$PW_{12}S/C_x/Al_2O_3$ catalysts were prepared by the incipient wetness technique via impregnation of the support (Al_2O_3 or C_x/Al_2O_3) with aqueous solutions containing the required amounts of 12-tungstophosphoric HPA $H_3PW_{12}O_{40} \times 3H_2O$, $NiCO_3$ and citric acid (all reagents are from Sigma–Aldrich, p.a.) with molar ratio citric acid/Ni = 1.5/1. The preparation proceeded as follows. First, a citric acid was dissolved in deionised water. $NiCO_3$ was slowly added to the citric acid solution and heated to 60–80 °C with stirring to achieve full dissolution. Next, the Ni-citrate solution was added to a $H_3PW_{12}O_{40}$ solution at the required concentration (Ni/W molar ratio was equal to 0.8) to prepare the impregnation solution. Subsequently, the supports were immersed in the impregnation solutions. All impregnated solids were aged at room temperature overnight and subsequently

Table 1
Composition and textural properties of prepared supports.

Support	Content in support		Textural characteristics		
	Carbon (wt.%)	Acid sites (μmol NH_3/g)	SSA[a] (m^2/g)	Pore volume (cm^3/g)	APR[b] (Å)
Al_2O_3	–	200	208	0.62	48
$C_{0.3}/Al_2O_3$	0.3	191	205	0.60	48
C_1/Al_2O_3	1.0	186	194	0.58	48
C_2/Al_2O_3	2.0	179	187	0.55	48
C_5/Al_2O_3	5.1	142	184	0.49	47

[a] Specific surface area.
[b] Average pore radius.

Table 2
Composition and textural properties of prepared catalysts.

Catalyst	Content in the catalyst (wt.%)		Textural characteristics		
	W	Ni	SSA[a] (m^2/g)	Pore volume (cm^3/g)	APR[b] (Å)
Ni_6-$PW_{12}S/Al_2O_3$	15.2	3.9	165	0.34	42/24
Ni_6-$PW_{12}S/C_{0.3}/Al_2O_3$	15.0	3.8	160	0.32	42/24
Ni_6-$PW_{12}S/C_1/Al_2O_3$	15.1	4.1	158	0.29	42/24
Ni_6-$PW_{12}S/C_2/Al_2O_3$	15.1	3.9	157	0.30	42/24
Ni_6-$PW_{12}S/C_5/Al_2O_3$	14.9	3.9	147	0.25	42/20

[a] Specific surface area.
[b] Average pore radius.

air-dried at 110 °C for 10 h without calcination. The theoretical contents of W and Ni in the catalysts were 15 and 3.9 wt.%, respectively.

The catalyst samples were activated by sulphidation for further analysis using physicochemical methods. A mixture of dimethyldisulphide (DMDS, 2 wt.% of sulfur) and decane at 3.5 MPa was utilized in a stepwise procedure conducted over 10 h at 240 °C and 8 h at 340 °C. Elemental analysis (W and Ni) was performed using an EDX800HS analyzer (Table 2).

2.2. Characterisation of catalysts

2.2.1. Textural characteristics of catalysts

The textural characteristics of the prepared catalysts were determined by nitrogen adsorption performed at 77 K on a Quantochrome Autosorb-1 adsorption porosimeter. The specific surface area (SSA) was calculated using the Brunauer–Emmett–Teller method at relative partial pressures (P/P_0) ranging from 0.05 to 0.3. The total pore volume and pore size distribution were calculated from a desorption curve using the Barret–Joyner–Halenda model at a P/P_0 of 0.99. Before the adsorption measurement the samples were outgassed under vacuum at 350 °C for 6 h and $p < 10^{-1}$ Pa.

2.2.2. X-ray diffraction (XRD)

XRD patterns were obtained with an ARLX'TRA powder diffractometer using Cu Kα radiation (λ = 1.54056 Å) at 38 mA, 43 kV and a scanning speed of 2 °/min. The diffractograms were analysed using standard JCPDS files.

2.2.3. Acidic properties of CCA supports

The acidity of the CCA supports was measured by temperature-programmed desorption of ammonia (NH_3-TPD) using TPDRO 1100 series multifunction adsorption instrument. The samples were outgassed in the He flow at 550 °C for 1 h. NH_3 adsorption was carried out at 60 °C in the NH_3 flow diluted with N_2 (1:1) and purified on a column with granulated NaOH. Complete saturation of the samples with ammonia was achieved within 30 min. Then weakly bounded NH_3 was removed by treating the samples in the dry He flow at 100 °C during 1 h. Next, the reactor was cooled to room temperature. A typical TPD experiment was run in the dry He flow (30 mL/min) with temperature being increased linearly from 25 to 750 °C and at the heating rate 8 °/min.

2.2.4. H_2 Temperature programmed reduction (H_2 TPR)

H_2-TPR was carried out on a TPDRO 1100 series multifunction adsorption instrument. A 0.1 g sample was pretreated in argon air at 110 °C for 3 h, after being cooled to room temperature, the sample was treated with 5% hydrogen in nitrogen at a constant flow rate of 50 mL/min, and heated to 1000 °C at the rate of 10 °/min. The signal reflecting the concentration of H_2 in H_2/N_2 variation was recorded by a thermal conductivity detector. Water produced in the course of reduction was adsorbed in a column filled by granulated NaOH.

2.2.5. High-resolution transmission electron microscopy (HRTEM)

HRTEM images of the catalysts were obtained on a Tecnai G2 20 electron microscope with a 0.14 nm lattice-fringe resolution and an accelerating voltage of 200 kV. The high-resolution images of the periodic structures were analysed using the Fourier method. Local energy-dispersive X-ray analysis (EDXA) was carried out on an EDXA spectrometer fitted with a Si (Li) detector with a 130 eV resolution. The samples used for HRTEM were prepared on a perforated carbon film mounted on a copper grid, and 10–15 representative micrographs were obtained for each catalyst in high-resolution mode. Typically, the lengths of at least 400 slabs were measured for each catalyst. To measure the extent of WS_2 dispersion, the average fraction of W atoms at the WS_2 edge surface (D) was calculated, assuming that the WS_2 slabs were perfect hexagons [10]. WS_2 dispersion (D) was statistically evaluated by dividing the total number of W atoms at the edge surface (W_e), including corner sites (W_c), by the total number of W atoms (W_T) using the slab sizes measured in the TEM micrographs:

$$D = \frac{W_e + W_c}{W_T} = \frac{\sum_{i=1..t} 6n_i - 6}{\sum_{i=1..t} 3n_i^2 - 3n_i + 1}, \quad (1)$$

where n_i is the number of W atoms along one side of the WS_2 slab, as determined by its length, and t is the total number of slabs in the TEM micrograph.

The number of slabs per stack was determined to obtain the average stacking degree ($\bar{N}$):

$$\bar{N} = \frac{\sum_{i=1..t} n_i N_i}{\sum_{i=1..t} n}, \quad (2)$$

where n_i is the number of stacks in N_i layers.

2.2.6. X-ray photoelectron spectroscopy (XPS)

The sulphided catalyst samples were analysed by XPS. The spectra were obtained on a Kratos Axis Ultra DLD spectrometer using a monochromatic AlK_a source (hν = 1486.6 eV, 150 W). The binding energy (BE) scale of the spectrometer was preliminarily calibrated using the position of the peaks for the Au $4f_{7/2}$ (83.96 eV) and Cu $2p_{3/2}$ (932.62 eV) core levels of pure metallic gold and copper. The samples were mounted on a holder using double-sided adhesive tape. For the non-conductive samples, the Kratos charge neutralizer system was used, and the spectra were charge-corrected to provide the C 1s spectral component of adventitious carbon (C—C, C—H) at 284.8 eV. In addition to the survey photoelectron spectra, narrow spectral regions (Al 2p, S 2p, W 4f, C 1s, O 1s and Ni 2p) were recorded. The pass energy of the analyzer was 160 eV for the survey spectra and 40 eV for the narrow scans. The individual spectral regions were analysed to determine the BE of the peaks, identify

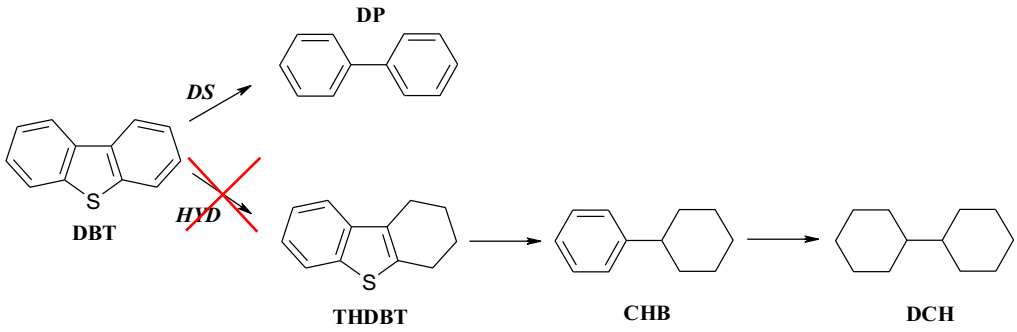

Scheme 1. Reaction network of the HDS of DBT.

the chemical state of the elements and calculate the relative ratios of the elements on the catalyst surface.

The collected spectra were analysed using the CasaXPS software program (Version 2.3.16) after applying a Shirley background subtraction. Gaussian (30%) – Lorentzian (70%) peaks were used for spectra decomposition. The decompositions of the S 2p, W 4f and Ni 2p XPS spectra were performed using the appropriate oxide and sulphided references as supported monometallic catalysts; the methodology for decomposing the spectra of NiW/Al_2O_3 catalysts was applied earlier, for instance [12,21,22].

XPS decomposition enabled the absolute quantification of each species:

$$C(j)_T(\text{at.}\%) = \frac{A_j/S_j}{\sum_{i=1..n} A_i/S_i} \times 100, \quad (3)$$

where A_i is the measured area of species i, S_i is the sensitivity factor of the atom related to species i (provided by the manufacturer) and $C(j)_T$ is the absolute content of species j. XPS sensitivity factors used in this work included the correction for the escape depth of the photoelectrons.

The relative concentrations of each species Ni^{2+}, NiS, NiWS, W^{6+}, WS_xO_y and WS_2 were determined for every sulphided catalyst. For example, the relative amount of NiWS was determined using the following equation:

$$[\text{NiWS}](\%) = \frac{A_{\text{NiWS}}}{A_{\text{NiWS}} + A_{\text{NiS}} + A_{\text{Ni}^{2+}}} \times 100, \quad (4)$$

where A_X represents the peak area of species x.

The effective Ni content in NiWS phase was determined using the following equation:

$$C_{\text{NiWS}} = [\text{NiWS}] \times C(\text{Ni})_T, \quad (5)$$

where $C(Ni)_T$ represents the effective concentration of cobalt determined by XPS (wt.%).

The promoter ratio in the active phase slab was determined using the following relation:

$$(\text{Ni/W})_{\text{slab}} = \frac{C_{\text{NiWS}}}{C_{WS_2}}, \quad (6)$$

where C_X is the absolute concentration of Ni (W) in the NiWS (WS_2) species (at.%).

The promoter ratio in the slab edge of the active phase was calculated as follows:

$$(\text{Ni/W})_{\text{edge}} = \frac{(\text{Ni/W})_{\text{slab}}}{W_e + W_c} \times W_T = \frac{(\text{Ni/W})_{\text{slab}}}{D}, \quad (7)$$

where D is the dispersion of the active phase obtained from TEM measurements.

The absence of any signal at 169.0 eV (characteristic of sulphates) indicates that sulphided catalysts were not reoxidised during the transfer of the solid from the sulphiding reactor to the XPS instrument.

2.3. Examination of the catalytic properties

The catalytic properties were determined using a fixed-bed microreactor featuring a high-pressure flow system. A 0.3 g sample of the catalyst (0.25–0.50 mm) was diluted with 1 cm^3 of low-surface-area carborundum (0.2–0.4 mm) and placed in the center of the reactor (the reactor had an internal diameter of 0.8 cm). Before testing, the catalysts were sulphided with a mixture of DMDS (2 wt.% of sulfur) and decane at 3.5 MPa in a stepwise procedure over 10 h at 240 °C and 8 h at 340 °C. A mixture of DBT (1500 ppm S), naphthalene (3 wt.%), quinoline (500 ppm N), hexadecane (as an internal standard, 1 wt.%) and toluene (as a solvent) was used as a model feedstock for evaluation of HDS, HYD and HDN performances. Catalysts were tested under the following conditions: 260 °C, 3.0 MPa hydrogen, 40–80 h^{-1} liquid hourly space velocity (LHSV) and a 500 NL/L volume ratio of hydrogen to feed. The liquid product compositions of the samples collected every 0.5 h were determined using a Crystall-5000 Gas Chromatograph equipped with a 30 m OV-101 column. The reaction products were identified by matching retention times with those of commercially available standards and by GC/MS analysis using a Finnigan Trace DSQ. The HDS reaction was allowed to proceed for 10 h to evaluate the deactivation of the catalyst. However, all catalysts exhibited stable performance, achieving a steady state after 5–6 h.

The rate constants of the pseudo-first-order reactions of the DBT HDS, naphthalene HYD and quinoline HDN were determined using the following equations:

$$k_{\text{HDS}} = -\frac{F_{\text{DBT}}}{W} \ln(1 - x_{\text{DBT}}),\ k_{\text{HYD}} = -\frac{F_{\text{Naph}}}{W} \ln(1 - x_{\text{Naph}}) \text{ and } k_{\text{HDN}} = -\frac{F_{\text{Qui}}}{W} \ln(1 - x_N) \quad (8)$$

where k_{HDS}, k_{HYD} and k_{HDN} are the pseudo-first-order reaction constants for the DBT HDS, naphthalene HYD and quinoline HDN (mol g^{-1} h^{-1}), respectively, x_{DBT}, x_{Naph} and x_N are the conversions (%) of DBT, naphthalene, quinoline and its nitrogen-containing products, respectively, F_{DBT}, F_{Naph} and F_{Qui} is the reactant flow in moles (mol h^{-1}) and W is the weight of the catalyst (g).

The HDS product from DBT included only biphenyl (BP) via the direct desulphurisation (DDS) pathway (Scheme 1). Absence of hydrogenated tetrahydro- and perhydrodibenzothiophenes, as well as cyclohexylbenzene (CHB) and bicyclohexyl (BCH) via the HYD pathway of DBT HDS was caused by strong inhibition effect of quinoline present in the feed. Tetralin, *c*- and *t*-decalines were the main products of naphthalene HYD reaction (Scheme 2). Since 90–95% quinoline rapidly turns into tetrahydroquinoline

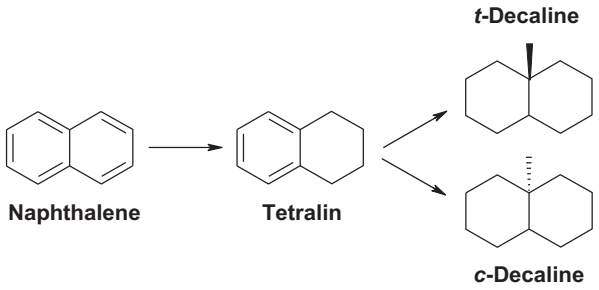

Scheme 2. Reaction network of the HYD of naphthalene.

(Scheme 3), conversion of nitrogen-containing compounds x_N was calculated as follows:

$$x_N = \frac{C_H}{C_H + C_N + C_{Qui}} \times 100\%, \quad (9)$$

where C_H is concentration (wt.%) of HDN products not containing nitrogen (propylbenzene (PB), propylcyclohexane (PCH)); C_N is concentration (wt.%) of HDN products containing nitrogen (tetrahydroquinoline (THQui), *o*-aminopropylbenzene (*o*-APB), *o*-aminopropylcyclohexane (*o*-APCH)); C_{Qui} is concentration (wt.%) of quinoline after reaction.

In order to explain changes in activities of the catalysts depending on characteristics of the species of the active phase NiWS, the turnover frequencies (TOF, s^{-1}) for the HDS of DBT, that for HYD of naphthalene and HDN of quinoline were calculated:

$$TOF_{HDS} = \frac{F_{DBT} \times x_{DBT} \times Mr_{Ni}}{W \times C_{NiWS} \times 3600}, TOF_{HYD} = \frac{F_{Naph} \times x_{Naph} \times Mr_{Ni}}{W \times C_{NiWS} \times 3600} \text{ and } TOF_{HDN} = \frac{F_{Qui} \times x_N \times Mr_{Ni}}{W \times C_{NiWS} \times 3600} \quad (10)$$

where F_{DBT}, F_{Naph} and F_{Qui} is the reactant flow in moles (mol h^{-1}); x_{DBT}, x_{Naph} and x_N are the conversions (%) of DBT, naphthalene, quinoline and its nitrogen-containing products, respectively, W is the weight of the catalyst (g), C_{NiWS} is the effective Ni content in NiWS phase (wt.%) and Mr_{Ni} is the molar mass of nickel (58.7 g/mol). This equation was used because of high excess of Ni content in the catalysts and much smaller TOF number of W^{IV} sites compared with promoted NiWS sites.

3. Results

3.1. Characteristics of the catalysts

The synthesized CCA supports containing carbon up to 5 wt.% inessentially differ in their textural properties (Table 1). With the carbon content growth, the SSA of the supports and specific pore volume correspondingly decreased from 208 to 184 m^2/g and from 0.62 to 0.49 cm^3/g. Average pore radius did not change and was equal 48 Å. Such textural changes are evidently determined by carburizing the alumina mesopores without formation of secondary coke pores. Saving average pore radius in CCA after alumina carbonization confirmed the uniform coke species distribution with graphitize state [54] and absence of large porous species. Indeed, our evaluations showed that the monolayer coverage of alumina could be achieved at 5 wt.% of the carbon content. An increase in the coke content reduced the total acidity of the CCA supports from 200 to 142 μmol NH_3/g (Table 1). The similar phenomena were observed earlier [54] and can be explained by formation of coke species on the acidic sites of the Al_2O_3 with their blocking.

The prepared Ni_6-$PW_{12}S/C_x/Al_2O_3$ catalysts remained similar to each other in composition and their textural characteristics (Table 2). Higher Ni/W molar ratio than values reported in [10,16,22,31] was chosen to obtain the catalysts with NiWS phase species, of which the WS_2 slabs would be fully decorated by Ni atoms. This allowed us to exclude different composition effect into NiWS phase species on catalyst performance. After sulphidation, the SSA and the specific pore volume decreased by ~20 and 50 rel.%, respectively, from those of the initial support (Fig. 1a). The average pore radius decreased by 6 Å and new mesopores with radius of 20–24 Å, probably belonging the coke species formed from citrate molecules, were detected (Fig. 1b).

The XRD patterns of the catalysts in oxide and sulphide states (not presented here) revealed only the low-temperature phase of the γ-Al_2O_3 support (PDF No. 48-367). Therefore, the XRD analysis of the prepared samples did not indicate the presence of any voluminous sulphides or oxides, suggesting that the W- and Ni-containing species were most likely amorphous and/or the crystallites were too small to generate XRD signals.

To investigate types and reducibility of active metals existing in the catalyst precursors H_2-TPR experiments were performed. Also, the reduction profiles of the oxide precursors provide useful information about the degree of interaction between the supported phases and the support. TPR experiments were carried out with the Ni_6-$PW_{12}/C_x/Al_2O_3$ catalysts in the oxide state. The TPR profiles are given in Fig. 2. To avoid the effect of the decomposing products of citric acid (CO, CO_2 and H_2O), the column filled by granulated NaOH as well as cooling trap were used in the experiments. Because of thermal conductivity of hydrogen is much higher than other gases the TPR peaks are indicated only hydrogen consumption. The TPR curves of all catalysts show three reduction peaks in the temperature ranges of 300–500 °C (L zone) and 530–700 °C (M zone), and one broad peak at higher 800 °C (H zone). Exact attribution of TPR signals over NiW catalysts is always complicated [16,55,61–65] because of the complex character of the reduction of W^{6+} oxide species, which proceeds through different intermediate oxidation states, depending on the reduction conditions, support nature, precursor type, etc. According to [66], W^{6+} species firstly reduced to W^{5+} and then to W^{4+} phase. It is known that octahedrally coordinated WO_x species are reduced at temperatures 300–600 °C [61], while tetrahedrally coordinated isolated or dimeric WO_x

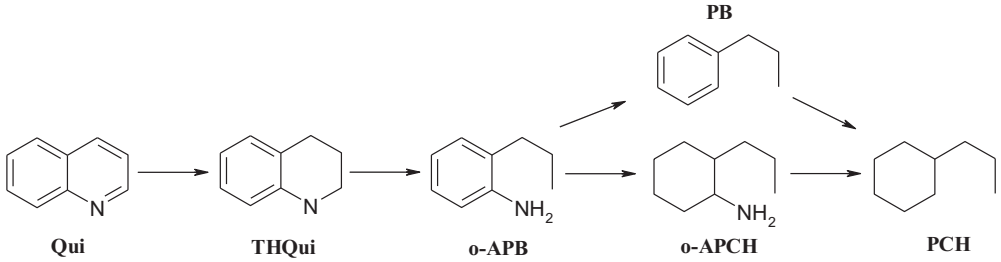

Scheme 3. Reaction network of the HDN of quinoline.

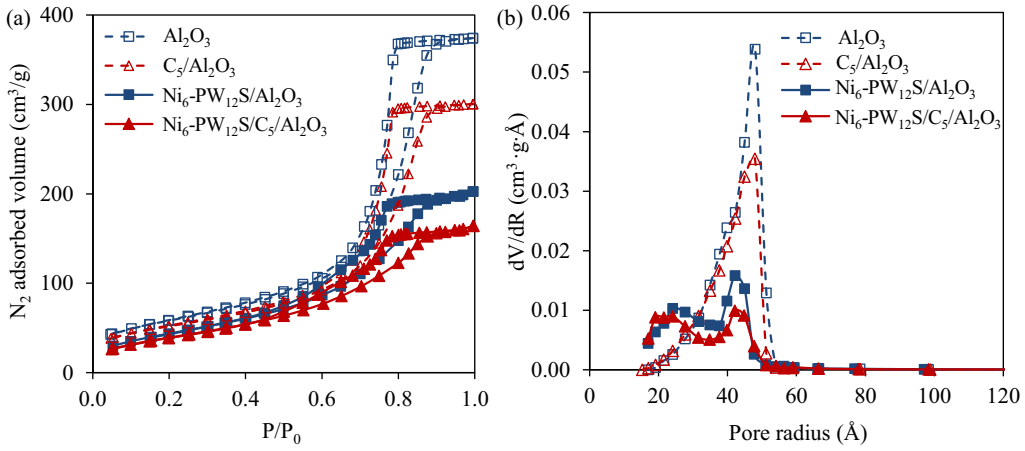

Fig. 1. N_2 adsorption–desorption isotherms (a) and BJH pores size distribution (b) of supports (open symbols) and sulfided catalysts (full symbols).

species with strong interaction with alumina are more difficult to reduce, requiring temperatures about 900–1000 °C [61,67,68]. It is shown [69,70] that nickel can form three types of species over alumina based catalysts: (i) bulk NiO with the reduction temperature ~400 °C, (ii) Ni^{2+}_{oct} species interacting with alumina with the reduction temperature of 450–690 °C, and (iii) Ni^{2+} incorporated into Al_2O_3, probably as $NiAl_2O_4$ spinel with the reduction temperature higher than 700 °C. Thus, the peak with maximum at ~380 °C (Fig. 2) is in TPR profiles of all catalysts. It corresponds to reduction of Ni^{2+} species [62] formed from decomposition of nickel citrate complexes. The peak at ~600 °C can be assigned to the superimposed reduction of polymeric octahedral W species and

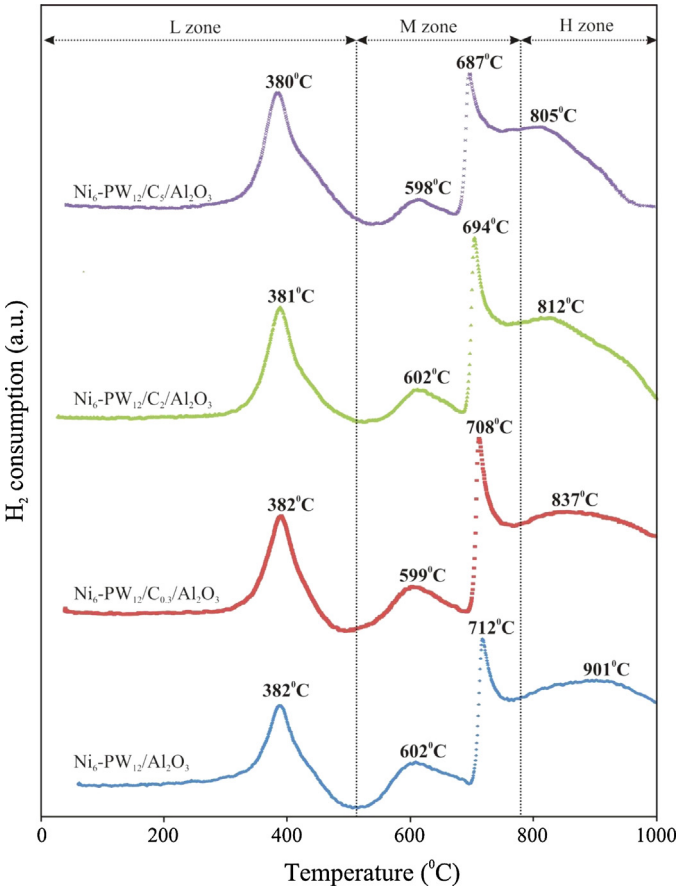

Fig. 2. TPR curves of Ni_6-$PW_{12}/C_x/Al_2O_3$ oxide catalysts.

Ni octahedral species (Ni^{2+}_{oct}) associated with the promotion of the active sulphided phase. The sharp peak at 700–730 °C corresponds to further reduction of W^{5+} species to W^{4+}, whereas the broad peak at higher temperatures (>800 °C) can be assigned to the reduction of tetrahedrally coordinated W^{4+} species to W^0 [62,69,70]. For CCA supports, the locations of two peaks of Ni_6-PW_{12}/Al_2O_3 catalysts at ca. 712 and 901 °C shifted toward lower temperatures (687 and 805 °C for Ni_6-$PW_{12}/C_5/Al_2O_3$ sample), demonstrating that metal oxide species have weaker interaction with the carbon-covered support. Therefore, covering alumina surface by coke is beneficial to tuning the metal-support interactions, which causes easier reduction of tungsten. Similar findings were also reported by Li et al. [55] for calcined $NiW/C/Al_2O_3$ catalysts with 0.45 wt.% carbon content, which were prepared with nickel nitrate and ammonium metatungstate as precursors.

Representative HRTEM micrographs of four sulphided Ni_6-$PW_{12}S/C_x/Al_2O_3$ catalysts are shown in Fig. 3. The black, thread-like fringes are the WS slabs. The fringes observed in the images were approximately 0.65 nm apart, matching the characteristic of (0 0 2) basal planes of crystalline WS_2. The HRTEM data allowed us to measure the average dimension of the NiWS phase particles, which varied from 4.4 to 5.6 nm, and the average stacking number in the WS_2 crystallites varied from 1.7 to 2.3 (Table 3). The distributions of the slab lengths and stacking numbers of the WS_2 particles are presented in Fig. 4. Using the CCA significantly altered the morphology of species of the active phase. The increase of carbon content up to 5 wt.% changed the average slab length from 4.4 to 5.6 nm. The average stacking number of the WS_2 crystallites increased from 1.7 to 2.3.

The chemical species present on the surface of the precursors and sulphided samples were evaluated by XPS (Fig. 5). Fig. 6 shows examples of decomposition of Ni 2p and W 4f photoelectron spectra recorded for Ni_6-$PW_{12}S/C_1/Al_2O_3$ catalyst. The spectral region of Ni $2p_{3/2}$ (Fig. 5a) contains three peaks with their respective satellites. The peak at a BE of 853.5 eV is related to NiWS phase. The signals at 852.4 eV and 856.3 eV correspond to the NiS species and Ni^{2+} in an oxidic environment, respectively [12,21,22,59,60]. The W 4f spectra (Fig. 5b) contain three W 4f doublets as follows: (1) a W $4f_{7/2}$ and $4f_{5/2}$ doublet with BE at 32.1 and 34.3 eV, respectively, associated with W^{4+} species of the WS_2 phase, (2) the doublet with binding energies at 33.2 and 35.2 eV related to W^{5+} species of a WS_xO_y oxysulphide species, and (3) finally the doublet with binding energies at 35.7 and 37.9 eV correlated with W^{6+} oxide species [12,21,22,59,60]. The decomposition of S 2p photopeaks (not presented here) evidenced two contributions assigned to sulphide (161.6 eV) and oxysulphide entities (163 eV).

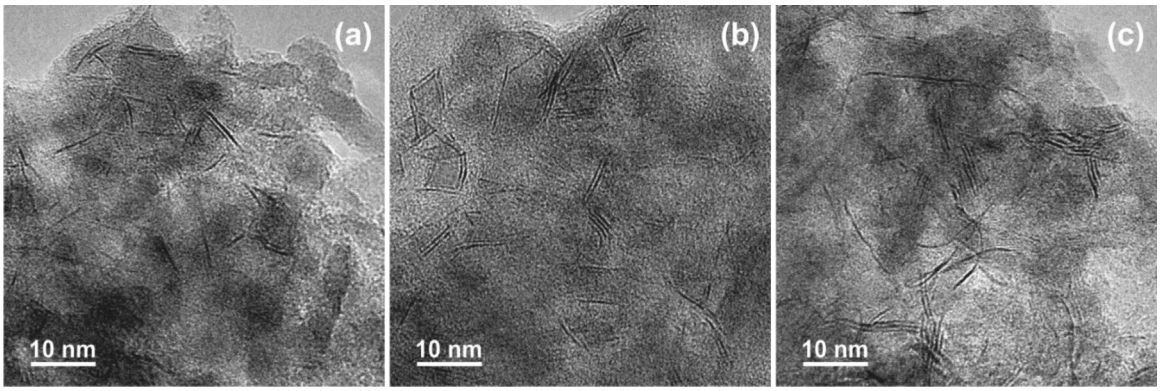

Fig. 3. HRTEM micrographs of sulfided Ni_6-$PW_{12}S/Al_2O_3$ (a), Ni_6-$PW_{12}S/C_2/Al_2O_3$ (b) and Ni_6-$PW_{12}S/C_5/Al_2O_3$ (c) catalysts.

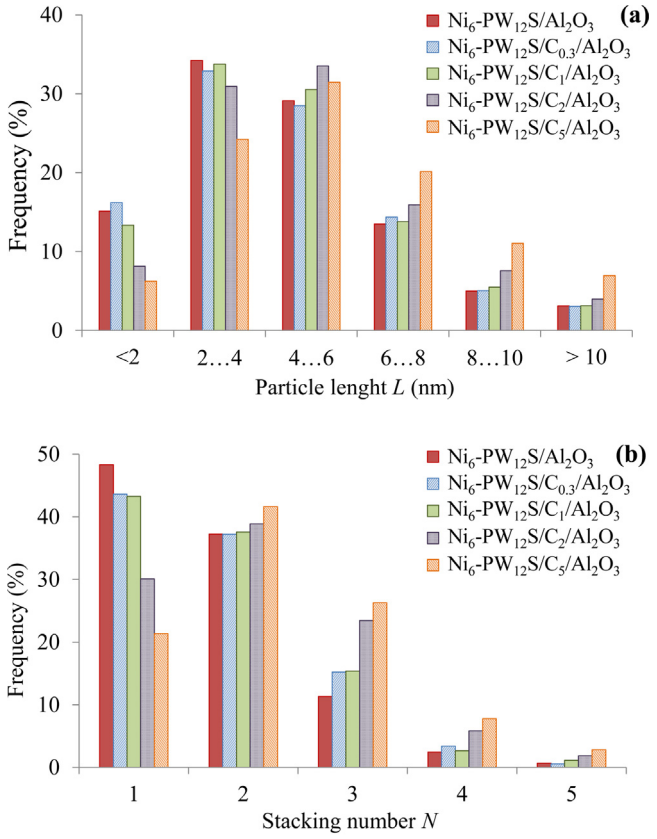

Fig. 4. Distributions of slab lengths (a) and stacking number (b) of WS_2 particles of Ni_6-$PW_{12}S/C_x/Al_2O_3$.

Table 3
WS_2 dispersion calculated from TEM micrographs.

Catalyst	Average length $\bar{L}$ (nm)	Average stacking number $\bar{N}$	Dispersion of WS_2 D[a]
Ni_6-$PW_{12}S/Al_2O_3$	4.4	1.7	0.27
Ni_6-$PW_{12}S/C_{0.3}/Al_2O_3$	4.4	1.8	0.27
Ni_6-$PW_{12}S/C_1/Al_2O_3$	4.5	1.8	0.26
Ni_6-$PW_{12}S/C_2/Al_2O_3$	4.9	2.1	0.24
Ni_6-$PW_{12}S/C_5/Al_2O_3$	5.6	2.3	0.22

[a] WS_2 dispersion calculated from HRTEM results (Eq. (1)).

The decomposition of the XPS spectra reveals the metal fractions for the nickel and tungsten species present on the surface of the sulphided Ni_6-$PW_{12}S/C_1/Al_2O_3$ catalysts (Table 4). In spite of using the liquid phase method for catalyst sulphidation, all samples had high content of tungsten presented as WS_2 (53–64%) that could be comparable with values for NiW catalysts sulphided by H_2S/H_2 in more severe conditions at 400 °C [12,21,22,59]. The increase of carbon content in the CCA led to rising the sulphidation degree of both metals (S/(Ni + W)), as well as NiWS, NiS and WS_2 percentages in Ni and W species. All catalysts had NiWS phase species with high promoting ratio $(Ni/W)_{edge}$ that was caused by excess of the promoter amount in the catalysts (Ni/(Ni + W) = 0.45). The obtained values $(Ni/W)_{edge}$ were sometimes higher than 1 (100% promotion) because of the uncertainties of the different values given by the TEM and XPS measurement and used for the calculations. Full promotion of NiWS edges by nickel was achieved in the catalysts supported on the CCA with carbon content equal 0.3 wt.% and more. However, sample with high carbon content Ni_6-$PW_{12}S/C_5/Al_2O_3$ had less Ni content in NiWS phase and $(Ni/W)_{slab}$ ratio than catalysts with 1 and 2 wt.% of carbon in support. This result can be explained by strong reduction of the dispersion of NiWS entities in Ni_6-$PW_{12}S/C_5/Al_2O_3$ catalyst.

Table 4
Metal fractions measured by XPS for nickel and tungsten species present at the surface of sulfided NiW/Al_2O_3 catalysts.

Catalyst	$\left(\frac{Ni}{W}\right)_{slab}$ [a]	$\left(\frac{Ni}{W}\right)_{edge}$ [b]	$\left(\frac{S}{Ni+W}\right)$	C_{NiWS}[c] (wt.%)	Ni fraction (rel.%)			W fraction (rel.%)		
					NiWS	NiS	Ni^{2+}	WS_2	WS_xO_y	W^{6+}
Ni_6-$PW_{12}S/Al_2O_3$	0.24	0.90	1.42	0.34	28	38	34	53	8	44
Ni_6-$PW_{12}S/C_{0.3}/Al_2O_3$	0.28	1.03	1.55	0.48	36	40	24	61	8	33
Ni_6-$PW_{12}S/C_1/Al_2O_3$	0.30	1.14	1.60	0.54	38	40	22	63	8	31
Ni_6-$PW_{12}S/C_2/Al_2O_3$	0.29	1.20	1.61	0.55	38	41	21	62	9	29
Ni_6-$PW_{12}S/C_5/Al_2O_3$	0.26	1.20	1.67	0.53	35	45	20	64	9	27

[a] Ni/W ratio in the NiWS slabs calculated from XPS results (Eq. (6)).
[b] Ni/W ratio in the NiWS edges calculated from XPS and HRTEM results (Eq. (7)).
[c] Effective Ni content in total NiWS phase species from XPS results (Eq. (5)).

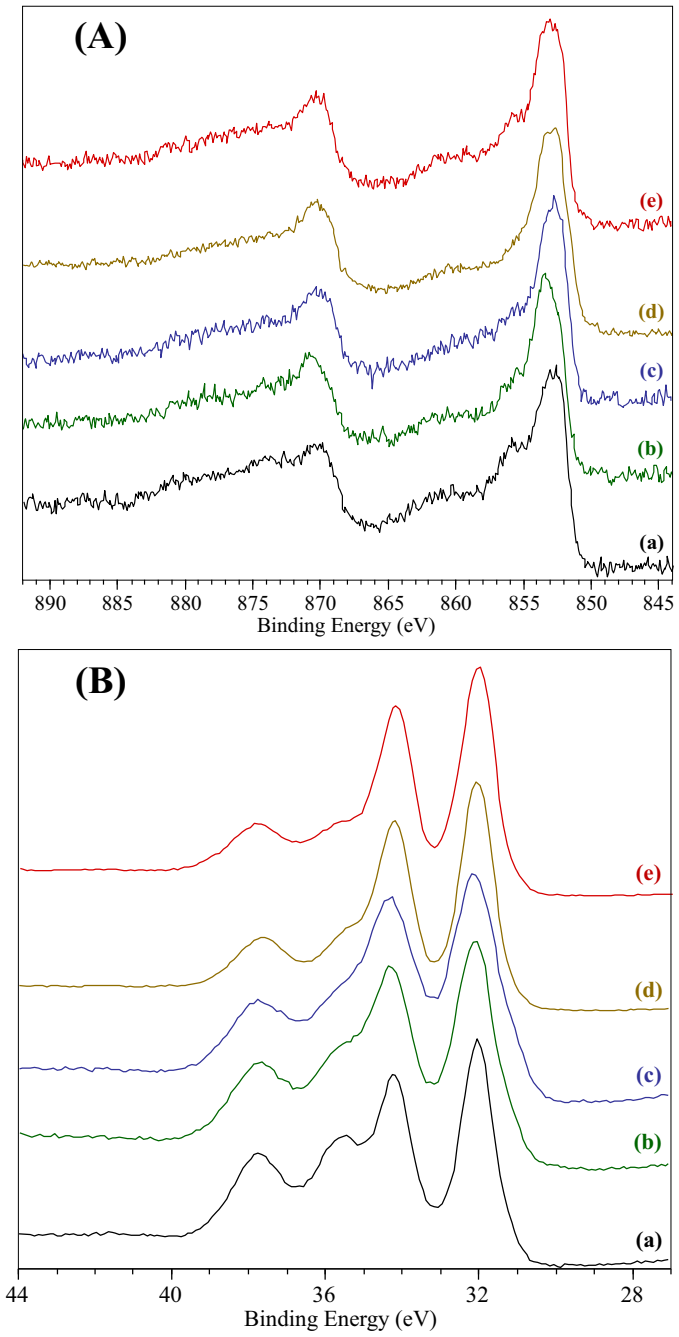

Fig. 5. XPS spectra of sulfided Ni_6-$PW_{12}S/C_x/Al_2O_3$ catalysts. (A) Ni 2p spectra, (B) W 4f spectra: (a) Ni_6-$PW_{12}S/Al_2O_3$, (b) Ni_6-$PW_{12}S/C_{0.3}/Al_2O_3$, (c) Ni_6-$PW_{12}S/C_1/Al_2O_3$, (d) Ni_6-$PW_{12}S/C_2/Al_2O_3$ and (e) Ni_6-$PW_{12}S/C_5/Al_2O_3$.

3.2. Catalytic properties

Table 5 shows the hydrotreating results for a mixture of DBT, naphthalene and quinoline. The conversion of all substrates in the course of the tests varied from 8.5 to 33%. Conversions of reactants depending on the reaction type increased in the order HDN ≈ HYD < HDS that correlated with the reactivity of the chosen compounds. Catalytic activities of the catalysts were essentially depended on the carbon content in the CCA-support. The catalyst supported on C_x/Al_2O_3 where x = 1 wt.% was the most active in all studied reactions (Fig. 7). Catalyst activities decreased at higher carbon content in CCA. These results were caused by close nature of the active sites for different reactions and similar inhibition effect of quinoline and its derivatives. On the other hand, it witnessed to the common reason of the changing of the catalyst properties. Rate constants depending on the reaction type increased in the order HDN « HDS ≈ HYD, whereas TOF values increased in the order HDN « HDS < HYD.

4. Discussion

Using the CCA as supports of the Ni_6-$PW_{12}S/C_x/Al_2O_3$ catalysts altered the morphology and structure of the particles of the NiWS active phase (Tables 3 and 5). With the rise of carbon content in the CCA, reducible reactivity (Fig. 2), sulphidation degree (Table 4), average length and stacking number of WS_2 crystallites (Table 3) increased. Observed changes can be explained by weakening interaction between metal oxide species and carbon-covered support. This property allowed the CCA supported catalysts to be deeper sulphided compared with Ni_6-$PW_{12}S/Al_2O_3$ one. On the other hand, weaker interaction with the support and better sulphidation reactivity of the precursors led to the formation of longer NiWS species having higher stacking number, i.e., lower dispersion. Similar findings were also reported by Li et al. [55] for calcined $NiW/C/Al_2O_3$ catalysts with 0.45 wt.% of carbon, which were prepared using nickel nitrate and ammonium metatungstate as precursors. Despite the fact that the authors did not vary the carbon content in the CCA, the $NiW/C/Al_2O_3$ catalyst had higher activity in HDS of 4,6-DMDBT than the reference NiW/Al_2O_3. However, these features differ from the ones obtained for $Ni(Co)Mo/C_x/Al_2O_3$ catalysts, which we investigated earlier [52,54]. In the case of Mo-based catalysts, the slab length dependence on the carbon content went through the minimum at 1.5–2 wt.% of carbon. It was explained by a change in surface density of carbon particles located on the alumina surface [54]. Probably, more difficult sulphidation of W-based catalysts than Mo-containing ones is caused by this difference. Improved sulphidation of the CCA supported catalysts provided higher effective Ni content in the NiWS active phase compared with the reference. However, maximal NiWS content (0.55 wt.%) was achieved at 1–2 wt.% of carbon in the support. Further increasing the carbon amount led to decrease in both effective Ni content and Ni percentage in the NiWS phase species. This falling probably caused by substantial reducing the dispersion of the NiWS particles. Since the Ni content in all catalysts was the same, decreasing the dispersion of the active phase

Table 5
Catalytic properties of prepared catalysts in hydrotreating of DBT, naphthalene and quinoline.

Catalyst	Conversion (%)			Rate constants ($\times10^{-4}$ mol h^{-1} g^{-1})			TOF values ($\times10^{-4}$ s^{-1})		
	DBT HDS	Naphthalene HYD	Quinoline HDN[a]	k_{HDS}	k_{HYD}	k_{HDN}	TOF_{HDS}	TOF_{HYD}	TOF_{HDN}
Ni_6-$PW_{12}S/Al_2O_3$	21.5	8.5	8.9	8.3	9.7	2.3	35 ± 1.6	44 ± 1.9	10.6 ± 0.6
Ni_6-$PW_{12}S/C_{0.3}/Al_2O_3$	28.0	10.0	10.0	11.3	11.5	2.6	33 ± 1.3	38 ± 1.5	8.6 ± 0.3
Ni_6-$PW_{12}S/C_1/Al_2O_3$	33.0	11.7	11.7	13.7	13.6	3.1	34 ± 1.5	39 ± 1.5	8.9 ± 0.4
Ni_6-$PW_{12}S/C_2/Al_2O_3$	32.0	11.0	10.8	13.2	12.7	2.9	33 ± 1.3	36 ± 1.4	8.1 ± 0.4
Ni_6-$PW_{12}S/C_5/Al_2O_3$	24.4	10.2	10.0	9.6	11.8	2.6	26 ± 1.1	35 ± 1.3	7.7 ± 0.3

[a] Conversion of quinoline and its N-containing products.

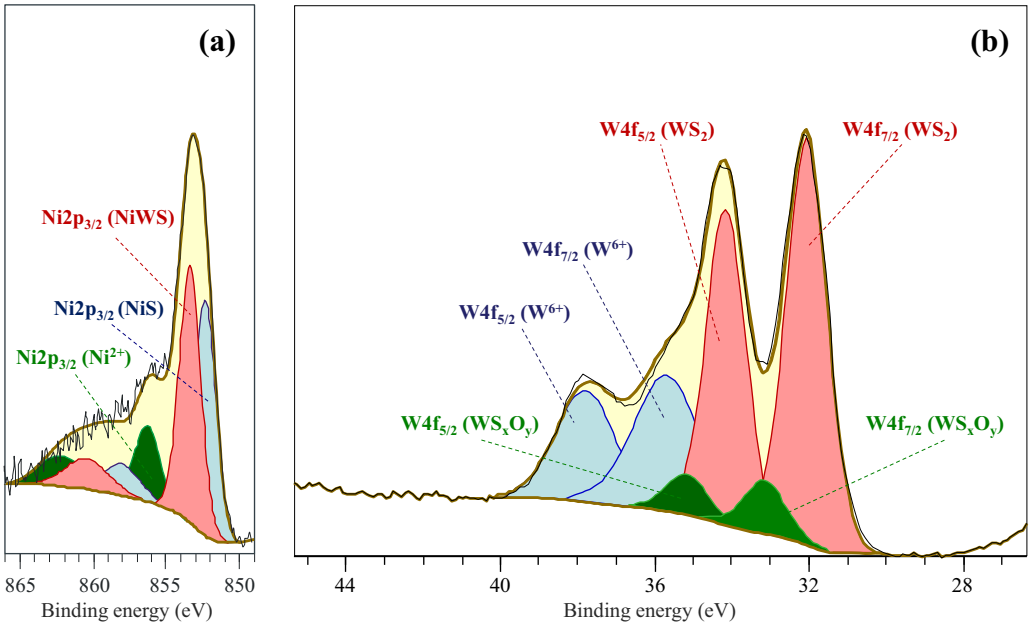

Fig. 6. Examples of decomposition of XPS Ni 2p (a) and W 4f (b) spectra recorded for Ni_6-$PW_{12}S/C_1/Al_2O_3$ catalyst; for (a) in green: Ni^{2+} oxide contributions; in blue: NiS contributions; in red: NiWS phase contributions; for (b) in blue: W^{6+} oxide contributions; in green: WS_xO_y contributions; in red: WS_2 contributions. (For interpretation of the references to color in this figure legend, the reader is referred to the web version of this article.)

particles to 0.22 (Table 3) limited location of the Ni atoms on the edges of WS_2 slabs with formation of the NiWS active phase. As a result, promoter atoms that cannot be fixed on fully promoted longer NiWS particles migrate to non-active NiS species in the Ni_6-$PW_{12}S/C_5/Al_2O_3$ catalyst. Attempts to observe any nickel sulfide species in sulphide catalysts by XRD or TEM were not successful. This indicated that NiS_x species were small and probably formed with amorphous coke.

Comparing the active phase morphology, the $(Ni/W)_{edge}$ ratio and catalytic properties of the CCA-supported NiW catalysts we found that TOF numbers in HDS, HYD and HDN linearly increased with the decrease of average length of the active phase particles (Fig. 8). Such dependences of activity on size of active phase particles were observed in [10,54,57] for Co(Ni)Mo catalysts and in [12,22,31,55,64,71] for NiW ones. However, sometimes [53,55,69,72] it is difficult to precisely ascertain the real cause of improving the catalytic activity due to simultaneous changing of several properties in the catalysts (length of the active phase and

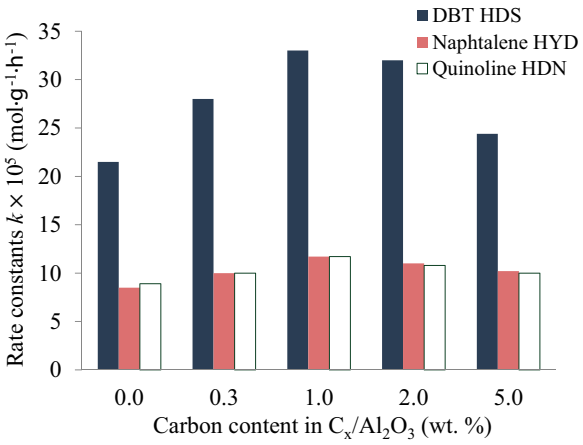

Fig. 7. Dependences of rate constants of HDS, HYD and HDN reactions of hydrotreating of DBT, naphthalene and quinoline over Ni_6-$PW_{12}S/C_x/Al_2O_3$ catalysts on carbon content in support C_x/Al_2O_3.

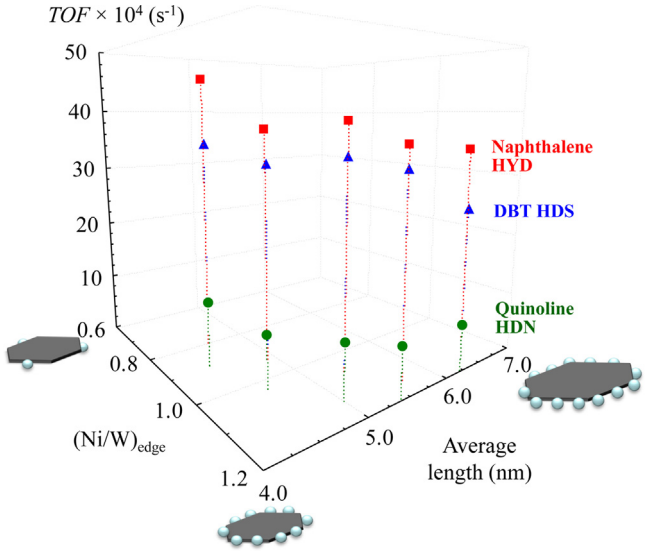

Fig. 8. 3D dependences of TOF number in HDS, HYD and HDN reactions of hydrotreating of DBT, naphthalene and quinoline over Ni_6-$PW_{12}S/C_x/Al_2O_3$ catalysts on average length of NiWS phase and $(Ni/W)_{edge}$ ratio.

stacking number of $Mo(W)S_2$, NiWS content, acidity of support, etc.). Fig. 8 also shows that the decrease of the $(Ni/W)_{edge}$ ratio in nano-sized NiWS species of Ni_6-$PW_{12}S/C_x/Al_2O_3$ catalyst is preferable for high TOF numbers. It should be noted, that the TOF numbers increased with the decrease in $\bar{L}$ at every constant $(Ni/W)_{edge}$ and vice versa. The samples with the lowest average length for the NiWS phase and smallest $(Ni/W)_{edge}$ ratio exhibited the highest TOF values. Therefore, in the HDS of DBT-derived molecules as well as the HYD of aromatic hydrocarbons and the HDN reactions over a multi-slab species of the NiWS active phase, two factors (average length of NiWS phase and $(Ni/W)_{edge}$ ratio) can exactly determine the catalytic activity. Marchand et al. [73] observed that adding Co or Ni to the edges of MoS_2 to achieve full coverage decreases the TOF during toluene HYD normalized by Co(Ni) edge site. The reduced amount

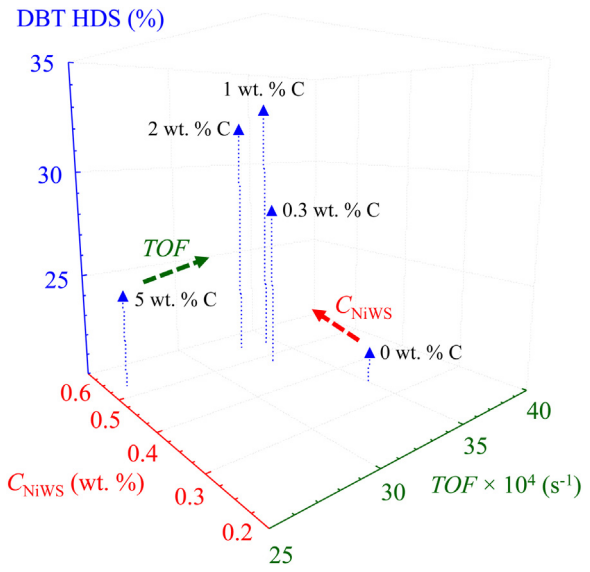

Fig. 9. 3D dependence of DBT conversion in HDS on effective Ni content in NiWS phase and TOF number for Ni_6-$PW_{12}S/C_x/Al_2O_3$ catalysts (legends at markers correspond to the carbon content in the CCA). Dotted lines show the ways of increasing DBT conversion.

of mixed sites may be attributed to the loss of intrinsic activity for promoter ratios above 0.3. Recently we also reported [56] that the TOF value for the DBT HDS over $CoMo/Al_2O_3$ catalysts decreased linearly as the Co/Mo ratio increased.

In this work, the reference catalyst Ni_6-$PW_{12}S/Al_2O_3$ had maximal TOF values in all reactions (Table 5) thanks to the lower average length of the species of NiWS phase and $(Ni/W)_{edge}$ value (Fig. 8). However, the depths of HDS, HYD and HDN reactions over this catalyst were not the highest (Table 5). The reason of this defect is in the lower Ni content in the NiWS phase than in the analogs (Table 4). Small amount of high active NiWS sites did not allow to the deep hydrotreating of model feedstock. Ni_6-$PW_{12}S/C_1/Al_2O_3$ catalyst produced maximal conversions of the substrates in studied reactions. This result achieved due to optimal balance between its TOF value of the active sites and their content (Fig. 9). It was shown that increase of carbon content in the CCA allowed to essentially increase the Ni content in NiWS phase, that led to producing of high-effective catalysts. In addition, it is necessary to note another role of carbon in the CCA supported catalysts. Earlier [52] kinetic measurements of benzene HYD suggested that a deficit of hydrogen limited catalytic activity at high temperatures. It was supposed that intermediate carbon placed between the alumina support and the active phase accumulated hydrogen inside carbon pores. Hydrogen accumulated inside carbon pores supplied active sites and, thereby, increased catalytic activity. Later [54] TPR measurements indicated hydrogen uptake by the C-coated support at reaction temperatures. It witnessed that CCA accumulated gas phase hydrogen and could be a source of hydrogen for hydrotreating reactions. However, the carbon amount in the CCA should be optimal. Excessive carbon content significantly decreased TOF values of active sites and their effectiveness in HDS, HYD and HDN reactions.

5. Conclusions

Using the CCA as supports of the Ni_6-$PW_{12}S/C_x/Al_2O_3$ catalysts altered the morphology and structure of the NiWS active phase. With the rise of carbon content in the CCA up to 5 wt.%, reducible reactivity, sulphidation degree, average length and stacking number of WS_2 crystallites in the catalysts increased. Observed changes can be explained by weakening interaction between metal oxide species and carbon-coated support. Therefore, covering alumina surface by coke is beneficial to tuning the metal-support interactions, which causes easier reduction of tungsten. This property allows the CCA supported catalysts to be deeper sulphided compared with the Ni_6-$PW_{12}S/Al_2O_3$ reference.

The increase of carbon content led to the rise of the average slab length and the average stacking number of the WS_2 crystallites from 4.4 to 5.6 nm and from 1.7 to 2.3, respectively. It was shown that the increase of carbon content in the CCA allowed to essentially increase the Ni content in NiWS phase, that led to producing of high-effective catalysts. Full promotion of NiWS edges by nickel was achieved in the catalysts supported on CCA with carbon content equal 0.3 wt.% and more. Activities of the catalysts in DBT HDS, naphthalene HYD and quinoline HDN were essentially depended on the carbon content in the CCA-support. Ni_6-$PW_{12}S/C_1/Al_2O_3$ catalyst showed maximal conversions of the substrates in studied reactions. This result achieved due to an optimal balance between TOF value of the active sites and their content.

Comparing the active phase morphology, the $(Ni/W)_{edge}$ ratio and catalytic properties of the Ni_6-$PW_{12}S/C_x/Al_2O_3$ catalysts it was found that TOF numbers in HDS, HYD and HDN linearly increased with the decrease of both the average length of the species of the active phase and the $(Ni/W)_{edge}$ ratio. Further improvements of supported NiW catalysts may be achieved by increasing the dispersion of the active phase species and optimizing the $(Ni/W)_{edge}$ ratio.

Acknowledgments

The work was supported by Ministry of education and science of Russian Federation (project 10.1516.2014/K). K.I. Maslakov acknowledges partial support from M.V. Lomonosov Moscow State University Program of Development.

References

[1] A. Stanislaus, A. Marafi, M.S. Rana, Catal. Today 153 (2010) 1.
[2] H. Topsøe, B.S. Clausen, F.E. Massoth, Catalysis–Science and Technology, in: J.R. Anderson, M. Boudart (Eds.), Hydrotreating Catalysis, vol. 11, Berlin-Heidelberg-N.Y., Springer-Verlag, 1996, p. 310.
[3] H. Topsøe, Appl. Catal. A 322 (2007) 3.
[4] M.S. Rana, R. Navarro, J. Leglise, Catal. Today 98 (2004) 67.
[5] S.A. Ali, M.A.B. Siddiqi, React. Kinet. Catal. Lett. 61 (1997) 363.
[6] W.R.A.M. Robinson, J.A.R. van Veen, V.H.J. de Beer, R.A. Santen, Fuel Proc. Technol. 61 (1999) 103.
[7] L. Coulier, V.H.J. Beer, J.A.R. Veen, J.W. Niemantsverdriet, J. Catal. 197 (2001) 26.
[8] K. Al-Dalama, B. Aravind, A. Stanislaus, Appl. Catal. A 296 (2005) 49.
[9] P. Mazoyer, C. Geantet, F. Diehl, S. Loridant, M. Lacroix, Catal. Today 130 (2008) 75.
[10] E.J.M. Hensen, P.J. Kooyman, Y. van der Meer, A.M. van der Kraan, V.H.J. de Beer, J.A.R. van Veen, R.A. van Santen, J. Catal. 199 (2001) 224.
[11] U. Usman, M. Takaki, T. Kubota, Y. Okamoto, Appl. Catal. A 286 (2005) 148.
[12] J.C. Mogica-Betancourt, A. Lopez-Benitez, J.R. Montiel-Lopez, L. Massin, M. Aouine, M. Vrinat, G. Berhault, A. Guevara-Lara, J. Catal. 313 (2014) 9.
[13] L. Ding, Z. Zhang, Y. Zheng, Z. Ring, J. Chen, Appl. Catal. A 301 (2006) 241.
[14] M. Breysse, C. Geantet, P. Afanasiev, J. Blanchard, M. Vrinat, Catal. Today 130 (2008) 3.
[15] E. Kraleva, A. Spojakina, K. Jiratova, L. Petrov, Catal. Lett. 112 (2006) 203.
[16] R. Palcheva, A. Spojakina, G. Tyuliev, K. Jiratova, L. Petrov, Kinet.Catal. 48 (2007) 847.
[17] O.V. Klimov, A.V. Pashigreva, M.A. Fedotov, D.I. Kochubey, Y.A. Chesalov, G.A. Bukhtiyarova, A.S. Noskov, J. Mol. Catal. A 322 (2010) 80.
[18] P. Blanchard, C. Lamonier, A. Griboval, E. Payen, Appl. Catal. A 322 (2007) 33.
[19] J. Mazurelle, C. Lamonier, E. Payen, D. Guillaume, Catal. Today 130 (2008) 41.
[20] C. Lamonier, C. Martin, J. Mazurelle, V. Harlé, D. Guillaume, E. Payen, Appl. Catal. B 70 (2007) 548.
[21] K.B. Tayeb, C. Lamonier, C. Lancelot, M. Fournier, A. Bonduelle-Skrzypczak, F. Bertoncini, Appl. Catal. B 126 (2012) 55.
[22] K.B. Tayeb, C. Lamonier, C. Lancelot, M. Fournier, E. Payen, A. Bonduelle, F. Bertoncini, Catal. Today 150 (2010) 207.
[23] P.A. Nikul'shin, A.V. Mozhaev, D.I. Ishutenko, P.P. Minaev, A.I. Lyashenko, A.A. Pimerzin, Kinet. Catal. 53 (2012) 620.
[24] N.N. Tomina, P.A. Nikul'shin, A.A. Pimerzin, Pet. Chem. 48 (2008) 92.

[25] P.A. Nikulshin, Yu.V. Eremina, N.N. Tomina, A.A. Pimerzin, Pet. Chem. 46 (2006) 371.
[26] P.A. Nikulshin, N.N. Tomina, A.A. Pimerzin, A. Yu Stakheev, I.S. Mashkovsky, V.M. Kogan, Appl. Catal. A 393 (2011) 146.
[27] H. Shimada, Catal. Today 86 (2003) 17.
[28] E. Furimsky, F.E. Massoth, Catal. Today 52 (1999) 381.
[29] E. Furimsky, Carbons and Carbon Supported Catalysts in Hydroprocessing, Royal Society of Chemistry, Cambridge, 2009, pp. 150.
[30] D. Laurenti, B. Phung-Ngoc, C. Roukoss, E. Devers, K. Marchand, L. Massin, L. Lemaitre, C. Legens, A.-A. Quoineaud, M. Vrinat, J. Catal. 297 (2013) 165.
[31] E.J.M. Hensen, Y. van der Meer, J.A.R. van Veen, J.W. Niemantsverdriet, Appl. Catal. A 322 (2007) 16.
[32] B. Scheffer, P.J. Mangnus, J.A. Moulijn, J. Catal. 121 (1990) 18.
[33] A.J. van der Vlies, G. Kishan, J.W. Niemantsverdriet, R. Prins, Th. Weber, J. Phys. Chem. B 106 (2002) 3449.
[34] A.J. van der Vlies, R. Prins, Th. Weber, J. Phys. Chem. B 106 (2002) 9277.
[35] F. Rodríguez-Reinoso, Carbon 36 (1998) 159.
[36] L.R. Radovic, Physicochemical Properties of Carbon Materials: A Brief Overview, in: P. Serp, J.L. Figueiredo (Eds.), Carbon Materials for Catalysis, John Wiley & Sons, Inc., Hoboken, NJ, USA, 2008, p. 44.
[37] J. Ramirez, S. Fuentes, G. Diaz, M. Vrinat, M. Breysse, M. Lacroix, Appl. Catal. 52 (1989) 211.
[38] S. Eijsbouts, J.J.L. Hinerman, H.J.W. Elzerman, Appl. Catal. 105 (1993) 53.
[39] S.M.A.M. Bouwens, F.B.M. Vanzon, M.P. Vandijk, A.M. Vanderkraan, V.H.J. Debeer, J.A.R. van Veen, D.C. Koningsberger, J. Catal. 146 (1994) 375.
[40] M. Kouzu, Y. Kuriki, F. Hamdy, K. Sakanishi, Y. Sugimoto, I. Saito, Appl. Catal. A 265 (2004) 61.
[41] H. Farag, I. Mochida, K. Sakanishi, Appl. Catal. A 194 (2000) 147.
[42] F. Severino, J. Laine, A. Lopez-Agudo, J. Catal. 188 (2000) 244.
[43] A.I. Dugulan, J.A.R. van Veen, E.J.M. Hensen, Appl. Catal. B 142 (2013) 178.
[44] E. Lopez-Salinas, J.G. Espinosa, J.G. Hernandez-Cortez, J. Sanchez-Valente, J. Nagira, Catal. Today 109 (2005) 69.
[45] P. Gheek, S. Suppan, J. Trawczynski, A. Hynaux, C. Sayag, G. Djega-Mariadssou, Catal. Today 119 (2007) 19.
[46] J.P.R. Vissers, F.P.M. Mercx, S.M.A. Bouwens, V.H.J. de Beer, R. Prins, J. Catal. 114 (1988) 291.
[47] C.A. Leon, A.W. Scaroni, L.R. Radovic, J. Colloid Interface Sci. 1 (1992) 148.
[48] L.F. Sharanda, Y.V. Plyuto, I.V. Babich, Y.A. Babich, J.A. Moulijn, Mendeleev Commun. 9 (1999) 95.
[49] C. Glasson, C. Geantet, M. Lacroix, F. Labruyere, P. Dufresne, J. Catal. 212 (2002) 76.
[50] S. He, C. Sun, H. Du, X. Dai, B. Wang, Chem. Eng. J. 141 (2008) 284.
[51] F. Liu, S. Xu, Y. Chi, D. Xue, Catal. Commun. 12 (2011) 521.
[52] P.A. Nikulshin, N.N. Tomina, A.A. Pimerzin, A.V. Kucherov, V.M. Kogan, Catal. Today 149 (2010) 82.
[53] S.K. Maity, J. Ancheyta, Catal. Today 150 (2010) 231.
[54] P.A. Nikulshin, V.A. Salnikov, A.V. Mozhaev, P.P. Minaev, V.M. Kogan, A.A. Pimerzin, J. Catal. 309 (2014) 386.
[55] H. Li, M. Li, Y. Chu, F. Liu, H. Nie, Appl. Catal. A 403 (2011) 75.
[56] P.A. Nikulshin, A.V. Mozhaev, A.A. Pimerzin, V.V. Konovalov, A.A. Pimerzin, Fuel 100 (2012) 24.
[57] P.A. Nikulshin, D.I. Ishutenko, A.A. Mozhaev, K.I. Maslakov, A.A. Pimerzin, J. Catal. 312 (2014) 152.
[58] P.A. Nikulshin, A.V. Mozhaev, K.I. Maslakov, A.A. Pimerzin, V.M. Kogan, Appl. Catal. B 158 (2014) 161.
[59] D. Zuo, M. Vrinat, H. Nie, F. Mauge, Y. Shi, M. Lacroix, D. Li, Catal. Today 93 (2004) 751.
[60] L. Coulier, G. Kishan, J.A.R. van Veen, J. Niemantsverdriet, J. Phys. Chem. B 106 (2002) 5897.
[61] V.M. Benitez, N.S. Figoli, Catal. Commun. 3 (2002) 487.
[62] S. Echeandia, P.L. Arias, V.L. Barrio, B. Pawelec, J.L. Fierro, Appl. Catal. B 101 (2010) 1.
[63] L.Y. Lizama, T.E. Klimova, J. Mater. Sci. 44 (2009) 6617.
[64] X. Tao, Y. Zhou, Q. Wei, G. Yu, Q. Cui, J. Liu, T. Liu, Fuel Process. Technol. 118 (2014) 200.
[65] A. Duan, Z. Gao, Q. Huo, C. Wang, D. Zhang, M. Jin, G. Jiang, Z. Zhao, H. Pan, K. Chung, Energy Fuels 24 (2010) 796.
[66] D.C. Vermaire, P.C. van Berge, J. Catal. 116 (1989) 309.
[67] V. Logie, G. Maire, D. Michel, J.L. Vignes, J. Catal. 188 (1999) 90.
[68] X.L. Yang, W.L. Dai, R. Gao, K. Fan, J. Catal. 249 (2007) 278.
[69] J.N. Diaz de Leon, M. Picquart, L. Massin, M. Vrinat, J.A. de los Reyes, J. Mol. Catal. A 363 (2012) 311.
[70] X. Zhu, P. Huo, Y. Zhang, D. Cheng, C. Liu, Appl. Catal. B 81 (2008) 132.
[71] G. Yu, Y. Zhou, Q. Wei, X. Tao, Q. Cui, Catal. Commun. 23 (2012) 48.
[72] G. Wan, A. Duan, Y. Zhang, Z. Zhao, G. Jiang, D. Zhang, Z. Gao, J. Liu, K.H. Chung, Energy Fuels 23 (2009) 3846.
[73] K. Marchand, C. Legens, D. Guillaume, P. Raybaud, Oil Gas Sci. Technol. 64 (2009) 719.